

Model Validation of a Complex Aerospace Structure

Amy E. Rice, Thomas G. Carne and David W. Kelton, Sandia National Laboratories, Albuquerque, New Mexico

A series of modal tests were performed to validate a finite-element model of a complex aerospace structure. Data were measured using various excitation methods to extract clean modes and damping values for a lightly damped system. Model validation was performed for one subassembly as well as for the full assembly to pinpoint the areas of the model that required updating and to better ascertain the quality of the joint models connecting the various components and subassemblies. After model updates were completed using the measured modal data, the model was validated using frequency response functions (FRFs) as the independent validation metric. Test and model FRFs were compared to determine the validity of the finite-element model.

A finite-element model was created for an aerospace structure using new in-house model creation tools designed to decrease the time from solid model to fully functional structural dynamics model. To ascertain that the model created with these tools was an accurate representation of the dynamics of the system, the model needed to be validated with test data. With previous knowledge that few models are accurate without some debugging and model updating, a series of modal tests were planned to be used for both model updating and model validation.

Several modal test methods were employed to gather mode shape information for updating the model and for generating frequency response functions (FRFs) to validate the model. Data were analyzed in the frequency band of 100-1000 Hz to bracket a test environment for the structure. Both impulse and random vibration inputs were used for testing.

After the model was updated to remove errors and calibrate unknown material and joint properties, the model was validated against test data. Two metrics were used, modal assurance criteria (MAC) and a visual comparison of FRFs from key locations within the structure.

Model

The aerospace structure consists of an exterior shell structure surrounding interior bracing that supports several brackets holding payloads. Figure 1 shows a simplified illustration of the structure. The bracing is attached to the exterior shell using a combination of rivets and welds that are not explicitly modeled. The brackets are attached to the bracing using bolted joints, which are represented in the model using one-dimensional spring elements. The payloads are bolted to the brackets, which are also represented in the model with springs. Forces were input into the structure at the exterior shell in the lateral direction and at each of the mounting feet at an angle of 30° from axial.

The finite-element model of the structure is composed of 400,000 second-order elements, a mix of hexes, quads and beams resulting in 5.6 million degrees of freedom. Two models were created and run. The first was the full model containing all components, and the second model was a subassembly of the full model – an empty shell containing the exterior shell, interior bracing and a portion of the brackets (but no payloads).

The modes and FRFs of the structure were calculated using Salinas, a massively parallel structural dynamics code developed

at Sandia National Laboratories.*¹ The shell model ran for 1 hour on 80 processors to compute 35 modes up to 1000 Hz. The full model ran for 3 hours on 150 processors to compute 150 modes up to 2000 Hz and FRFs from four input locations.

Test Program

Two separate dynamics tests were conducted on the

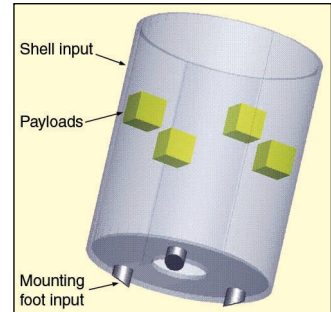


Figure 1. Simplified illustration of structure.

data for calibration and validation of the model. To develop an understanding of the structural dynamics of the base system that would drive a first round of updates to the model, the first test was conducted on a stripped-down version of the entire system. All payloads and most of the brackets were removed from the shell structure. This decision allowed some critical calibration of parameters that would have been more difficult if testing had only been performed at the full system. The second test was performed on the full structure with all the payloads and brackets in place. FRFs were recorded on both tests and used as validation data for the full system. Modal parameters, including the frequencies, damping, and shapes were extracted and compared with the model predictions.

Before any of the dynamic tests were performed, however, several mass properties measurements were conducted in which the mass, center of gravity, and mass moments of inertia were measured and compared with analytical predictions. These tests were simple, inexpensive, and accurate. Mass measurements were also made of various components and subassemblies as required. This data were extremely valuable in finding errors and omissions in the analytical model.

As noted, the first structure was basically an empty aerospace shell and fairly lightly damped, because most of the energy-dissipating interfaces had been removed. On this structure, the shell was excited with impacts using a modal impact hammer.² These inputs produced very clean FRFs with little obvious noise and good coherence functions. Several force-amplitude levels were used and produced nearly identical FRFs, showing that any nonlinearity of the system, at least at these “modal” levels of excitation, was not present in the measurements.

Three different input locations were chosen to excite all of the modes. Because the shell structure was primarily an axisymmetric structure, shell modes should appear in pairs with the two shapes rotated with respect to each other so that they would be orthogonal. There were no apparent principal directions to the shell to align inputs, so input locations were arbitrarily chosen at 0 and 45 degrees on the upper edge of the shell structure. Using inputs 45 degrees apart would assure that both pairs of the two-lobed and three-lobed shell ovaling modes would be excited. This input may only excite one of the four-lobed shell ovaling modes, but the analysis indicated that the four-lobed modes were outside the frequency band of interest. The third input was applied to the interior bracing to excite modes that had strong responses in that portion of the structure. Approximately 30 modes were extracted from the measured FRFs of the model, up to 1400 Hz, using the SMAC algorithm.³

The second test used the full structure with all its payloads and brackets. The damping for this structure increased over the bare

Based on a paper presented at IMAC XXVI, the 26th International Modal Analysis Conference, Society for Experimental Mechanics, Orlando, FL, February 4-7, 2008.

*Sandia National Laboratories is a multiprogram laboratory operated by Sandia Corporation, a Lockheed Martin Company, for the U.S. Department of Energy under Contract DE-AC04-94AL85000.

Models are prone to errors, incorrect assumptions, oversimplifications and unknown parameters. Some of these uncertainties can only be corrected through testing and model calibration.

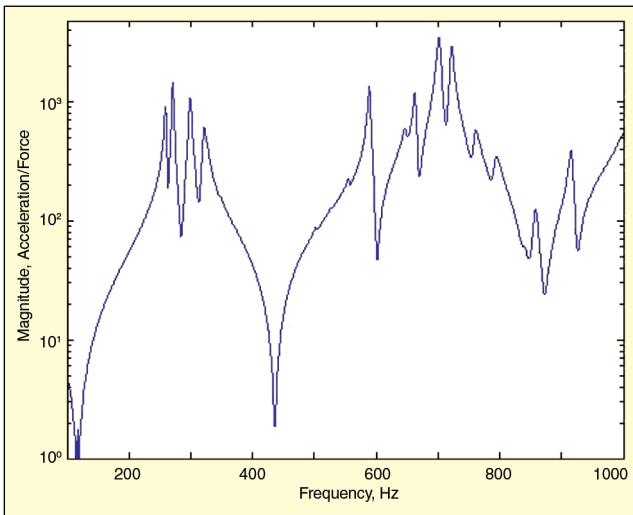


Figure 2. Measured driving point FRF for the shell input.

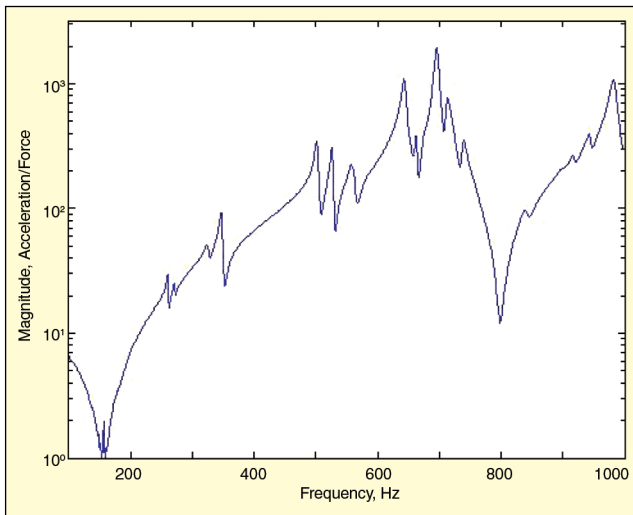


Figure 3. Measured driving point FRF for Mounting Foot 1 input.

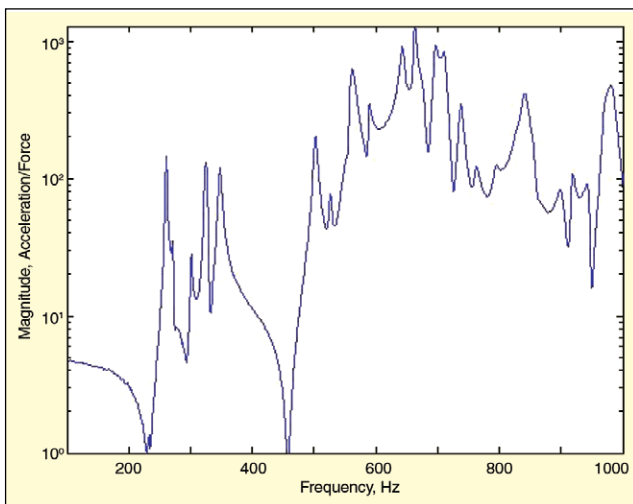


Figure 4. Measured payload response FRF for Mounting Foot 1 input.

shell tested initially, but was still fairly lightly damped with modal damping ratios generally between 0.5 and 1%. For this test, small modal shakers were used to excite the structure at a number of locations, using continuous random input with Hanning windows. Long time records were measured to minimize the effect of the Hanning window on the measured damping. The shaker input was specifically chosen to minimize any potential nonlinearities at the bolted joints in the assembly; the random vibration input would produce the best FRF fits to a linear system.⁴ In addition, since

the FRF data would be used for validation, the input locations and directions needed to be accurately constrained; this would have been more difficult using an impact hammer.

Four different inputs were applied to the structure independently, measuring FRFs for each input. In retrospect, it would have been better to have insisted that all inputs were applied simultaneously, but due to logistic constraints, the inputs were applied one at a time. This resulted in more complicated data analysis and some compromise to the data consistency. The structure has three mounting feet that attach it to the launch vehicle, and off-axis inputs were applied at these three locations. The fourth input was applied normal to the shell structure to excite the various shell modes. There was less concern about exciting shell modes in this test, since the shell modes had been characterized in the previous test.

Only three of the four sets of FRFs, the shell input and two of the three mounting feet inputs, were used to extract modal data. The modal parameters from the three inputs would be used to calibrate or update the model, leaving the fourth set of FRFs for validation data. A total of 28 modes was extracted between 0 and 1000 Hz, with the lowest frequency being 259 Hz. As mentioned previously, the damping ratios varied between 0.5 and 1% and were input into the analytical model. Mode shapes were measured with 39 tri-axial accelerometers, dispersed between several rows on the shell, interior bracing, brackets and payloads. These mode shapes were used to align the test modes with the analysis modes and produce MAC matrices that will be included in the validation discussion.

The driving-point FRF for the second test, with the input normal to the shell, is shown in Figure 2. The magnitude of the FRF is plotted from 100 to 1000 Hz, the frequency range of a test environment for the structure. This particular input produced very clean FRFs with distinct resonant frequencies and very little noise. The shell on this aerospace structure was very linear in its response. Interestingly, for this frequency range, the modes are clustered into two bands, one from 250 to 320 Hz and the second band from 550 to 750 Hz. The first band is basically shell modes with the payloads participating, while the second band of modes is dominated by payload and brackets interacting with the shell. Descriptions of mode shapes are included in Table 2.

The driving-point FRF input at Mounting Foot 1 is plotted in Figure 3 below with the same axes as Figure 2. This FRF has a different appearance, but certainly appears very noise-free. The low frequency shell modes are not nearly so evident in this FRF, but other modes are revealed, particularly around 500 Hz.

Figure 4 shows a response FRF on one of the payloads due to input at Mounting Foot 1. In this FRF, the low-frequency shell modes are amplified over that of the driving-point FRF, and it certainly appears that most of the modes in the overall band are excited to some degree. The deep antiresonance that appears at 800 Hz in the driving point does not show up in this response FRF. In fact, there appears to a very strong mode excited just about 800 Hz, which is barely noticeable in the driving-point functions.

Model Update

Ideally, a finite-element model would be error free and predictive upon creation. But in reality, models do contain errors, some of which are fairly easy to spot and others that require more effort to discover and correct. There are also some modeling parameters that require some type of test data to resolve. To find and correct these errors and define unknown properties, the finite-element model was updated in three stages. Prior to testing the actual hardware, the model was exercised and updated. After test data were available from each of the two modal tests, the model was again updated.

Before examining any test data, initial checkout of the model uncovered several modeling and material errors. The first step was to review the input deck for material properties and shell thicknesses. This check found one incorrect material property that was corrected. The second step was to compare the mesh to both the solid model and the actual hardware to verify that nothing important was omitted in the geometry simplification step. This check found one of the payloads was omitted along with several connectors that add stiffness and mass to otherwise empty cavities in the structure.

The third step was to calculate the mass of the structure and compare it to the mass of the actual hardware. The mass of the model was within 2% of the mass of the actual hardware, so there were no model changes as a result. The fourth step was to calculate the first 20 modes and animate them to check connectivity and look for anything unusual. Many connectivity issues were found at this stage, brackets not completely connected to bracing, bracing not connected to outer shell. And some low-frequency modes suggested that oversimplification of the bracing structure had reduced the stiffness of the structure. Some previously omitted details were added to stiffen the structure.

The first set of experimental modal data was measured for the aerospace structure without the payloads or payload brackets, providing validation data on a simpler structure than the full system. Animations were created of each of the modes and qualitatively compared to animations from the analysis to determine the matching modes. The frequencies were then compared to generate an error associated with each matching analysis mode. The first mode of the system is a 2,0 ovaling mode. The major player in that mode is the exterior shell, which consists of two stiff materials with a soft adhesive sandwiched in between. Although the bulk properties of the adhesive were known, incomplete adhesion to the other shell materials puts some uncertainty into the effective modulus. This value was calibrated to correlate the analysis ovaling modes to the test modes. Errors in the modes for the interior bracing were reduced after measuring the hardware and matching the bracing plate thicknesses in the model to the thicknesses of the actual hardware. Since there was only one piece of hardware available, it was impossible to collect statistical data on the piece-to-piece variation. Test and analysis modes are compared in Table 1. The biggest improvements in the model came from improving the value for the adhesive modulus.

A second set of modal data was taken for the entire system, which consisted of the exterior shell, interior bracing and payloads on brackets. As was done with the shell subassembly data, animations were made of each of the modes and qualitatively compared to analysis animations to determine the matching modes for the full system. The frequencies of the matching modes were compared and an error calculated. The initial comparison of frequencies indicated that there was a problem with the payloads. The lowest payload mode in the analysis was significantly lower than the test mode. The payloads were weighed, and an error was found in the density of the mass mock parts used in the analysis. The same error was repeated in all the payloads in the system. (The payloads were all modeled as solid blivets rather than as more complex

Table 1. Analysis mode updating – aerospace shell.

Mode Description	Test Freq., Hz	Anal. Freq. Before, Hz	Error Before	Anal. Freq. After, Hz	Error After
2.0 Ovaling	290	260	-10%	293	1.0%
2.0 Ovaling	294	263	-11%	297	1.0%
Bracket axial	334	365	9%	320	-4.1%
Bracket axial	404	471	17%	415	2.8%
Aft Hole 2,0 ovaling	607	740	22%	601	-1.0%
Aft Hole 2,0 ovaling	622	785	26%	616	-1.0%
3.0 ovaling	667	539	-19%	644	-3.4%
3.0 ovaling	683	542	-21%	665	-2.7%
Top bracing rocking	760	704	-7%	762	0.3%
Top bracing rocking	769	706	-8%	763	-0.8%

assemblies.) Most of the error was removed from the system with these corrections, but another uncertainty was the stiffness of all of the bolted connections on the brackets. Softening the joint stiffnesses brought the analysis error down to a very acceptable level. Test and analysis modes are compared in Table 2.

In addition to material and joint properties, damping ratios could only be determined through testing. The damping values for each test mode were used in the finite-element model when calculating FRFs for the system.

Model Validation

FRFs were collected for inputs made at four locations on the aerospace structure, at the three mounting feet and at one location on the exterior shell. Modal data from two of the mounting feet and from the exterior shell were used for updating the model; the data from the third mounting foot were used for the model validation. Two metrics were used for validation, the MAC was calculated for the test vs. analysis modes, and the FRFs were qualitatively compared at several locations within the structure.

The MAC matrix is shown in Figure 5. The chart indicates good modal correlation in the first four modes between the analysis and testing. The analysis calculated a fifth mode that wasn't measured in the test, so the fifth test mode matches the sixth analysis mode. The fifth analysis mode is a second axial mode with different phasing for the individual payloads, located fairly close in frequency to the other axial mode. It is likely that these modes had similar shapes and frequencies. So the fifth test mode was deleted because it had a high MAC (similar shape) compared to the sixth test mode, and they were indistinguishable.

Higher frequency modes do not show as high a MAC between test and analysis shapes, and some of the test modes appear to be linear combinations of several analysis modes. This is a common phenomenon with shell ovaling modes, since they do not have a preferred orientation. So the test and analysis modes may be shifted in orientation with respect to each other. It is also common for shell modes and payload modes to be out of phase with each other, especially at higher frequencies when there's more motion within the structure. Figure 6 is another MAC matrix calculated to allow linear combinations of all modes within $\pm 10\%$ of the frequency of the closest analysis mode.⁵ The MAC improves substantially for the higher frequency modes of the structure when linear combinations of analysis modes are allowed. Note that the analysis modes numbered in Figure 6 are linear combinations of the original analysis modes numbered in Figure 5.

The visual FRF comparison is a bit more challenging. A first

Table 2. Analysis mode updating – full system.

Mode Description	Test Freq., Hz	Anal. Freq. Before, Hz	Error Before	Anal. Freq. After, Hz	Error After
2.0 ovaling/payloads in phase with shell	259	173	-33%	261	0.7%
2.0 ovaling/payloads in phase with shell	271	175	-35%	273	0.6%
2.0 ovaling/payloads out of phase with shell	299	257	-14%	301	0.6%
2.0 ovaling/payloads out of phase with shell	321	280	-13%	322	0.4%
Payloads axial	348	236	-32%	356	2.2%
One payload rocking	527	406	-23%	535	1.5%
3.0 ovaling/all payloads out of phase with shell	644	618	-4%	644	0.0%
3.0 ovaling/2 payloads out of phase with shell	678	634	-6%	672	-0.9%
3.0 ovaling/2 payloads out of phase with shell	696	657	-6%	694	-0.3%
3.0 ovaling/2 payloads out of phase with shell	702	698	-1%	678	-3.5%
3.0 ovaling/2 payloads out of phase with shell	722	717	-1%	739	2.3%

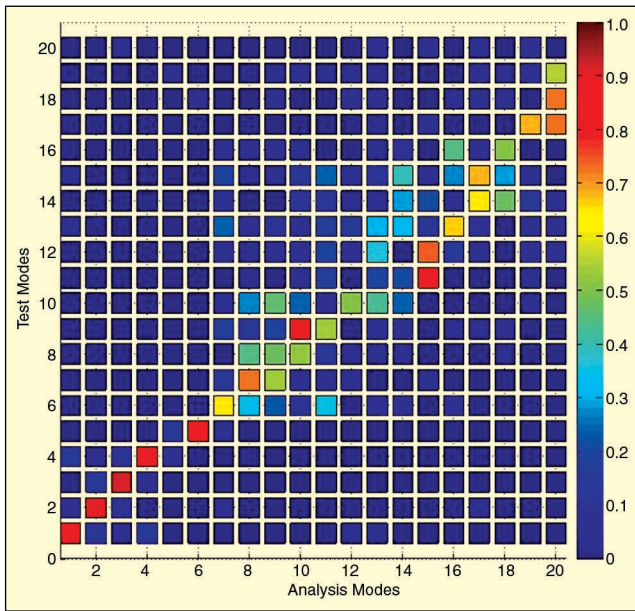


Figure 5. Mode assurance criteria matrix.

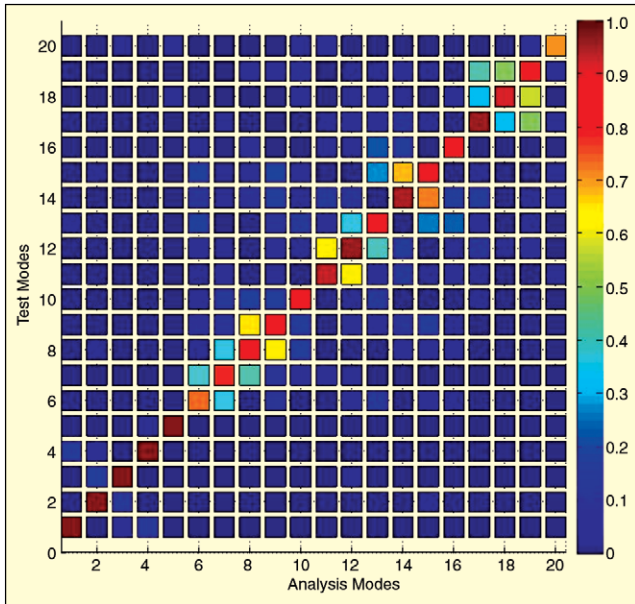


Figure 6. Mode assurance criteria with linear combination of modes within $\pm 10\%$.

comparison is the driving-point FRF, the acceleration output at the input location. Figure 7 shows the driving-point FRF for input on the exterior shell. The two data sets match almost exactly up to 500 Hz; however, at higher frequencies the test and analysis FRFs show the same general trends, but the modal peaks do not align. Overall, this is a very good fit for the model, especially considering the complexity of the structure. Driving-point FRFs taken at the three mounting points indicate an error in either the test or analysis data, or perhaps a boundary condition improperly represented in the finite-element model. So they are not presented here.

The next data of interest are the FRFs at one of the payloads. Figures 8 and 9 show the FRFs in the axial and lateral directions for one of the payloads with input from the third mounting foot. Similar to the driving point FRF, there is good correlation between the analysis and test data below 500 Hz, but above 500 Hz, there is a reasonable match to the trend of the test data although the modes again do not align.

Figures 10 and 11 show the FRFs at the same payload location as the previous two figures but generated from the lateral input into the exterior shell. Both FRFs do a better job of matching the test data than the previous FRFs calculated from the mounting foot. The shell input location is at a geometrically simpler section of the

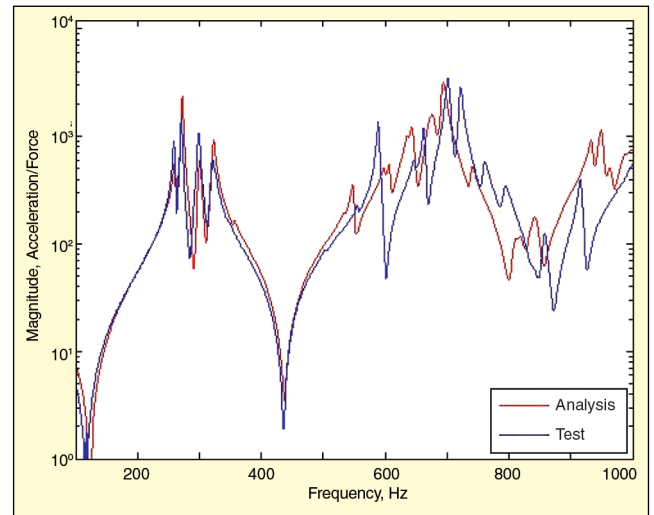


Figure 7. Driving-point frequency response function – lateral shell input.

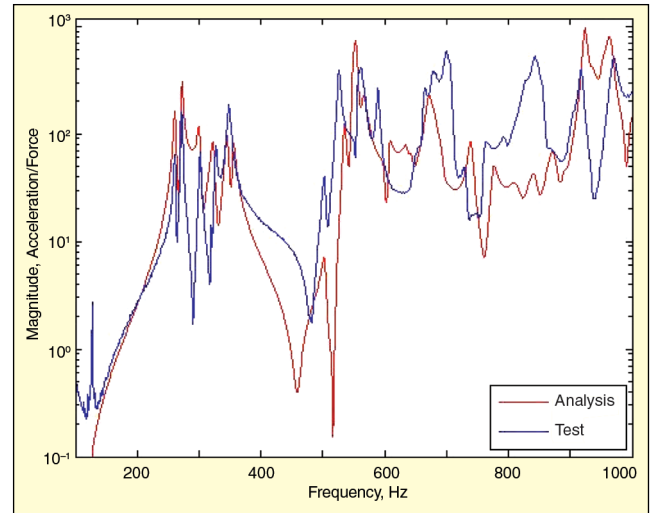


Figure 8. Axial response at payload to Mounting Foot 3 input.

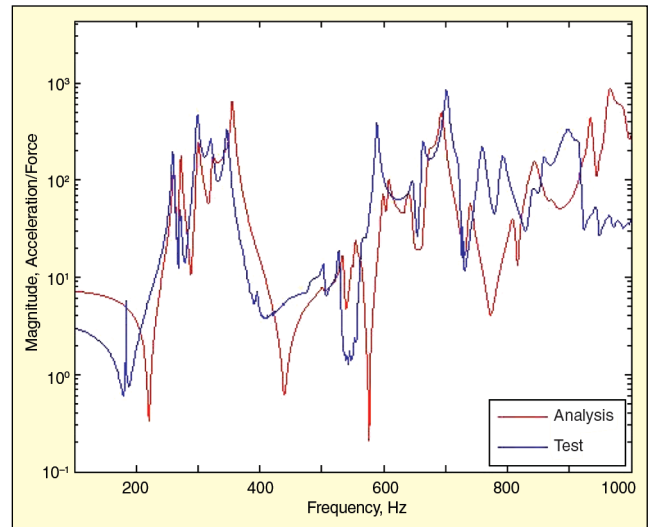


Figure 9. Lateral response at payload to Mounting Foot 3 input.

structure than the mounting feet. The mounting feet are test fixtures attached to the actual mounting locations of the structure, located close to many connector cavities with reinforcement features and other details, some of which were represented in the model in a simplified form and some of which were omitted completely. So an input location with less complexity, or less uncertainty, tends to yield cleaner matches between analysis and test data.

A visual comparison of FRFs is more qualitative than quantitative

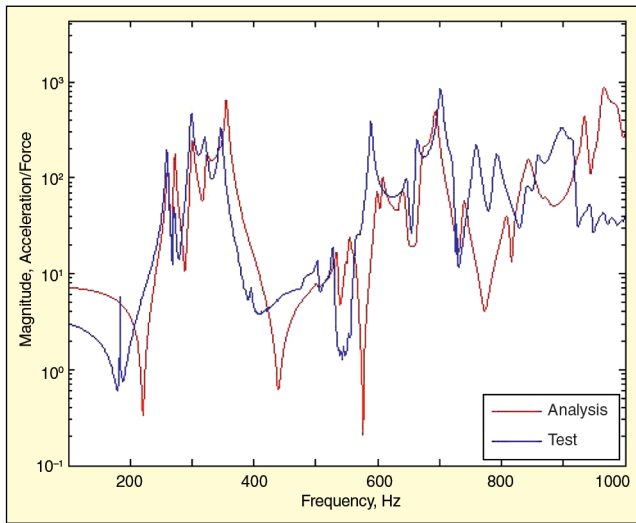


Figure 10. Axial response at payload to lateral shell input.

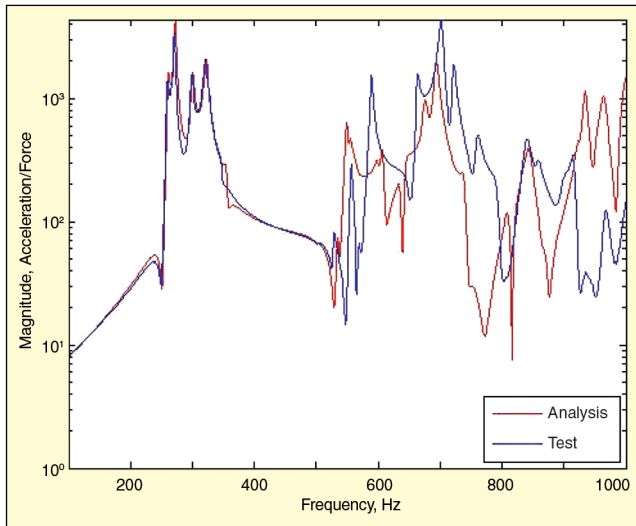


Figure 11. Lateral response at payload to lateral shell input.

tive. Many methods have been developed to quantify the data fit, but that discussion is beyond the scope of this article. As one can see, even a very good match of modal frequencies between the analysis and test data does not guarantee a good match of the FRFs. For the FRFs to correlate, one must have very good shape and damping matches as well. The shapes coefficient must match at both the input and output locations for good correlation of the FRFs. Comparing FRFs is a much more demanding validation metric than just comparing modal frequencies and MACs. However, the FRF comparison does reveal how well the model can predict responses due to a broad-band input or a single frequency input.

Conclusions

The model validation of this aerospace structure required a number of separate procedures. Initially, the model was updated with a four-step process without examining any test data. Many modeling errors and oversimplifications were corrected in this initial checkout, particularly connectivity issues. Then a stripped-down structure was examined and tested to simplify the correlation and to more easily isolate individual modeling issues. Various material parameters were calibrated during this step. Finally, the modal test data from the full structural system were used to compare modal frequencies and shapes. This revealed still more modeling issues and allowed further parameter calibration. It would be nice to have an accurate and predictive model out of the box, but this is rarely the case. Models are prone to errors, incorrect assumptions, oversimplifications and unknown parameters. Some of these uncertainties can only be corrected through testing and model calibration.

The two validation metrics for this model were the MAC calculations and the comparison of several key frequency FRFs using test data not used in the model-update step. The MAC calculation provided a good feeling about the modal correlation, but the FRFs revealed the response of components due to force inputs over the full frequency range. Using FRFs as the validation metric is very demanding but also conveys much more information about both the physical structure and the model.

The model did not include damping, only mass and stiffness; so the damping was extracted from the test data and used in the model for computing FRFs. Previously measured damping data from similar structures could have been used, but that is still a limiting aspect of the model.

Finally, we emphasize that the test data and model correlation are only representative of a single unit of a set of nominally identical structures known from previous experience to have unit-to-unit variability. Consequently, the uncertainty that has been shown here in the FRF comparisons must also be supplemented with some unit-to-unit uncertainty.

References

1. Bhardwaj, M., Pierson, K., Reese, G., Walsh, T., Day, D., Alvin, K., Peery, J., Farhat, C., and Lesoinne, M., "Salinas: A Scalable Software for High-Performance Structural and Solid Mechanics Simulations," Supercomputing 2002, Baltimore, MD, November 2002.
2. Carne, T. G., and Stasiunas, E. C., "Lessons Learned in Modal Testing, Part 3: Transient Excitation for Modal Testing, More than just Hammer Impacts," *Experimental Techniques*, Vol. 30, No. 3, pp. 69-79, May/June 2006.
3. Hensley, D. P., and Mayes, R. L., "Extending SMAC to Multiple References," Proceedings of the 24th International Modal Analysis Conference, pp. 220-230, February 2006.
4. Mayes, R. L., and Gomez, A. J., "Lessons Learned in Modal Testing, Part 4: What's Shakin', Dude? Effective use of Modal Shakers," *Experimental Techniques*, Vol. 30, No. 4, pp. 51-612, July/August 2006.
5. Simmermacher, T. W., and Tipton, D. G., Personal Communication, October 2007. 

The author can be reached at: aerice@sandia.gov.